PHYSICAL REVIEW A VOLUME 3, NUMBER 2 FEBRUARY 1971

Atomic Radiation Transition Probabilities to the 1s State and Theoretical K-Shell Fluorescence Yields*

Vaclav O. Kostroun
Ward Reactor Laboratory, Department of Applied Physics, Cornell University, Ithaca, New York 14850

and

Mau Hsiung Chen and Bernd Crasemann
Department of Physics, University of Oregon, Eugene, Oregon 97403

(Received 20 August 1970)

Radiationless transition probabilities to the atomic 1s shell are calculated for all transitions that contribute measurably to the Auger effect. Screened nonrelativistic hydrogenic wave functions are used. The effective charge for the continuum-electron Coulomb wave function is taken to be the geometric mean of the effective charges appropriate for the state from which the electron originates and the next-higher state. The results are combined with Scofield's radiative transition probabilities to derive theoretical K-shell fluorescence yields. Agreement with a selected set of most reliable ω_K measurements is very good in the range from $Z = 10$ to 55, and total K-level widths agree very well with measured values.

I. INTRODUCTION

Atomic fluorescence yields have gained interest in recent years because of their importance in pure atomic physics and in applications.[1] Radiationless transition rates are more sensitive to the detailed nature of the wave functions than many other measurable atomic quantities. Fluorescence yields are necessary for the interpretation of many nuclear and atomic measurements. Moreover, a precise knowledge of fluorescence yields is required for the accurate calculation of photon transport processes and for the design of shields and of many radiation detection devices. A comprehensive effort to derive fluorescence yields from theory is justified at the present time because rather numerous precise measurements have become available and have been critically evaluated,[2] and because accurate calculations of radiative transition probabilities have been accomplished.[3]

In the present paper, we show that K-shell fluorescence yields and widths in very good agreement with the best experimental results can be computed for a wide range of atomic numbers ($10 \leq Z \lesssim 55$) by combining Scofield's radiative widths[3] with radiationless transition probabilities calculated from nonrelativistic hydrogenic wave functions, provided that (a) a suitable screening rule for the continuum wave function is introduced and (b) all contributing transitions from outer shells are meticulously included. In a subsequent paper,[4] we work out Coster-Kronig transition probabilities and certain L-subshell fluorescence yields.

II. THEORY

A. Ansatz

Radiationless transitions are auto-ionization processes that arise from the electrostatic interaction between two electrons in an atom that initially is singly ionized in an inner shell. The basis of the quantum-mechanical theory of radiationless transitions was formulated by Wentzel.[5] The transition probability is given by the familiar formula of perturbation theory:

$$w_{fi} = (2\pi/\hbar)\left| \int \psi_f^* V \psi_i \, d\tau \right|^2 \rho(E_f), \tag{1}$$

where

$$V = \sum_{i \neq j} \frac{e^2}{r_{ij}},$$

and $\rho(E_f)$ is the density of final states for the energy E_f that satisfies conservation of energy. This expression has to be summed over all possible final states.

After a radiationless transition filling a single inner vacancy, the atom is left doubly ionized in inner shells. The states of such nearly-closed-shell configurations with two holes can be expressed in terms of completely-closed-shell configurations together with the correlated two-electron configurations.[6] In fact, in LS coupling the electrostatic energies are the same for the two systems.[7] The initial and final states can therefore conveniently be represented by the two-electron configurations correlated to two-hole configurations that consist (initially) of one inner-shell vacancy and one hole in the continuum, and (finally) of two inner-shell vacancies.

The direct matrix element occurring in Eq. (1) then is of the form

$$D = \iint \psi_a^*(1)\psi_b^*(2) \frac{e^2}{|\vec{r}_1 - \vec{r}_2|} \psi_c(1)\psi_d(2) \, d\tau_1 \, d\tau_2. \tag{2}$$

Here, ψ_b is a continuum wave function, while ψ_a,

ψ_c, and ψ_d are bound-state wave functions. The one-electron wave functions of the initial and final states are assumed to be orthogonal. This assumption is justified by the small difference between the self-consistent fields of the initial and final configurations.[8,9] The exchange matrix element E is similar to D [Eq. (2)], except that electron 1 is in state ψ_d and electron 2 is in the state ψ_c. The transition probability per unit time is

$$w_{fi} = (2\pi/\hbar)|D - E|^2 \rho(E_f). \tag{3}$$

If the continuum wave function ψ_b is adjusted to yield one electron ejected per unit time,[10,11] then $\rho(E_f) = h^{-1}$ and the transition probability becomes

$$w_{fi} = (1/\hbar^2)|D - E|^2. \tag{4}$$

This formula has been used in the calculations of Burhop[12] and in subsequent work.

B. Wave Functions

In first approximation, the electrons in bound states can be represented by single-particle wave functions in a central potential. We use nonrelativistic screened hydrogenic wave functions.[13] Such functions have been used in Burhop's pioneering work[12] and by Callan in his calculations of K-LL Auger transition probabilities[14-16] and of L_1-$L_{23}M_{45}$ Coster-Kronig transition rates,[17,18] as well as by others. Relativistic hydrogenic wave functions were first employed by Massey and Burhop[19] and most recently by Chattarji and Talukdar.[20,21] Added realism and sophistication can, in principle, be attained by using self-consistent-field (SCF) numerical wave functions[22-26] or analytic solutions of the wave equation for an approximate SCF potential, as done recently by McGuire.[27,28] However, the advantages of using simple analytic wave functions are obvious and, for the purpose of calculating fluorescence yields, results apparently can be at least as satisfactory as those derived from other approaches. This somewhat surprising result may be due to the fact that the main contribution to the Auger matrix element comes from intermediate distances from the nucleus, where the hydrogenic approximation is quite good.

For the continuum electron, we use a screened Coulomb wave function, normalized to one electron emerging per unit time[11,14,29]:

$$\psi_{\infty k} = \left(\frac{m}{\hbar}\right)^{1/2} \frac{2^{k+1}}{(2k+1)!}\, e^{\pi Z^*/2\kappa}\, \kappa^{k+1/2} \left|\Gamma\left(k+1+\frac{iZ^*}{\kappa}\right)\right| r^k e^{-i\kappa r} \times {}_1F_1\left(k+1+\frac{iZ^*}{\kappa};\ 2k+2;\ 2i\kappa r\right) Y_{km}(\theta,\varphi). \tag{5}$$

Here, ${}_1F_1(a;b;c)$ is the confluent hypergeometric function, κ is the wave number of the ejected electron, k is the orbital angular momentum quantum number of the ejected electron, and Z^* is the effective charge, discussed in Sec. II C.

C. Screening

The importance of choosing an appropriate effective charge $Z^* = Z - \sigma$ is well-known; the result depends critically upon this choice.[14,18] For the bound-state wave functions, we follow the Hartree recipe[30] and let $\sigma = Z - (\langle r_H\rangle/\langle r\rangle)$. Here, $\langle r_H\rangle$ is the mean hydrogenic radius and $\langle r\rangle$ is the mean Hartree-Fock radius. We use $\langle r\rangle$ as computed by Froese for neutral atoms.[31]

It is more difficult to select an appropriate effective charge for the continuum electron which sees a steadily decreasing charge as it moves away from the nucleus. We find that best results are obtained if Z^* in the continuum wave function is taken to be the geometric mean of the effective charge appropriate for the state from which the continuum electron originates and the effective charge pertaining to the next-higher state. Thus, for the K-$L_{23}M_{23}$ transition, for example, the effective charge in the continuum wave function is $[Z^*(3p)\cdot Z^*(3d)]^{1/2}$ for the direct and $[Z^*(2p)\cdot Z^*(3s)]^{1/2}$ for the exchange matrix element.

D. Evaluation of Radial Matrix Elements

Separation of the matrix element (2) into radial and angular factors is accomplished by expressing the Coulomb interaction potential in terms of scalar products of irreducible tensor operators[32,33]:

$$\frac{1}{r_{12}} = \sum_{\nu,\sigma} \gamma_\nu(r_1, r_2)\, C^*_{\nu\sigma}(\Omega_1)\cdot C_{\nu\sigma}(\Omega_2), \tag{6}$$

where

$$\gamma_\nu(r_1, r_2) = \begin{cases} r_1^\nu / r_2^{\nu+1}, & r_1 < r_2 \\ r_2^\nu / r_1^{\nu+1}, & r_2 < r_1 \end{cases} \tag{7}$$

$$C_{\nu\sigma} = \left(\frac{4\pi}{2\nu+1}\right)^{1/2} Y_{\nu\sigma}(\Omega), \tag{8}$$

the $Y_{\nu\sigma}$ being spherical harmonics.

The direct radial matrix elements then are of the form

$$\{(n''l'')|(nl)(n'l'),\nu,k\} = e^2 \int_{r_1,r_2=0}^{\infty} \gamma_\nu R_{n''l''}(r_1) R_{nl}(r_1) R_{n'l'}(r_2) R^k_\infty(r_2) r_1^2 r_2^2\, dr_1\, dr_2. \tag{9}$$

Here, the R's are radial wave functions that describe states characterized by the quantum numbers identified in Fig. 1. The notation is that of Asaad and Burhop[6]; the quantum numbers $n''l''$ are suppressed when there is no chance for confusion. The derivation of an explicit general expression for the radial matrix elements is outlined in Appendix A.

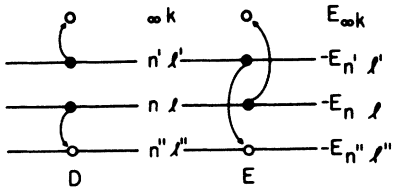

FIG. 1. Schematic representation or direct (D) and exchange (E) Auger processes, illustrating the notation used to designate quantum numbers that characterize the pertinent states.

E. Coupling: Angular Factors

Evaluation of the angular factors in the matrix elements (2) depends upon a choice of the appropriate angular-momentum coupling scheme. If spin-orbit coupling is neglected, the initial and final two-hole states of the atom can be expressed for different values of the total angular momentum J in the $LSJM$ representation of Russell-Saunders coupling. For the heavier atoms, this is not a good approximation, because the spin-orbit interaction outweighs the electrostatic interaction, and inner-shell electron states are described more realistically by j-j rather than LS coupling. If one is interested in the relative intensities of the various radiationless transitions leading to a given final-state configuration, as in Auger-electron spectroscopy, it is important to choose the appropriate coupling scheme for each range of atomic numbers. Thus, calculations have been carried out in LS coupling,[14,22] extreme j-j coupling,[24,25] and intermediate coupling.[6,26] However, if the purpose of the calculation is merely to determine the *total* radiationless transition probability into a certain final-state configuration (regardless of the term) in order to determine fluorescence yields, then it does not matter what coupling scheme is chosen, as long as the initial vacancy is not in the final configuration. The total transition rate is independent of the coupling because the wave functions in the various schemes are related by unitary transformations.

The relation between j-j and LS wave functions is discussed in Appendix B, where attention is called to an important class of transitions for which total rates are most conveniently evaluated in j-j coupling. However, for the calculations with which the present paper deals, it is possible and easiest to express the transition rates in LS coupling, and we restrict ourselves to this scheme.

In $LSJM$ representation, the antisymmetrized and properly normalized two-particle wave functions are of the form[32]

$$\psi_A(n_a l_a, n_b l_b; SLJM)$$

$$= 2^{-1/2} \sum_{M_L M_S} (SM_S LM_L | JM)[\varphi(n_a l_a n_b l_b LM_L)$$

$$+ (-)^{l_a+l_b-L+S}\varphi(n_b l_b n_a l_a LM_L)]\chi(\tfrac{1}{2}\tfrac{1}{2}Sm_S), \quad (10)$$

where

$$\varphi(n_\alpha l_\alpha n_\beta l_\beta LM_L) = \sum_{m_\alpha m_\beta} (l_\alpha m_\alpha l_\beta m_\beta | LM_L)\varphi_1(l_\alpha m_\alpha)\varphi_2(l_\beta m_\beta) \times R_1(n_\alpha l_\alpha)R_2(n_\beta l_\beta), \quad (11)$$

$$\chi(\tfrac{1}{2}\tfrac{1}{2}SM_S) = \sum_{m_s m_{s'}} (\tfrac{1}{2} m_s \tfrac{1}{2} m_{s'} | SM_s)\chi_1(m_s)\chi_2(m_{s'}). \quad (12)$$

Here, $\varphi_i(l_j m_j)$, $R_i(n_j l_j)$, and $\chi_i(m_{s'})$ are the single-particle angular, radial, and spin-wave functions of electron i, with quantum numbers n_j, l_j, m_j, and $m_{s'}$.

The total transition probability into all possible states of L and S for a given final configuration of the atom then is

$$w = \sum_{L,S} \frac{(2S+1)(2L+1)}{2(2l''+1)} \times \sum_k \left| \frac{1}{\hbar}\langle n''l'' \infty kSLJM \left| \frac{e^2}{r_{12}} \right| nln'l'SLJM\rangle \right|^2, \quad (13)$$

where the single-particle radial wave functions are normalized; they are denoted by their quantum numbers as defined in Fig. 1. Equation (13) is summed over the magnetic quantum numbers of the final atom and the orbital angular momentum k of the ejected electron, and averaged over the quantum numbers of the initial vacancy.

Separation into radial and angular factors, as discussed in Sec. IID, leads to

$$w = \sum_{S,L} \frac{(2S+1)(2L+1)}{2(2l''+1)} \sum_k \left| \frac{1}{\hbar} \sum_\nu [d_\nu D_\nu \pm (-)^{l+l'} e_\nu E_\nu] \right|^2, \quad (14)$$

where the plus sign goes with even $L+S$ and the minus sign with odd $L+S$.

The functions D_ν and E_ν are the direct and exchange radial matrix elements $\{(n''l'') | (nl)(n'l'), \nu, k\}$ and $\{(n''l'') | (n'l')(nl), \nu, k\}$ discussed in Sec. IID and Appendix A. The angular factors d_ν and e_ν are as follows:

$$d_\nu = (-)^{l+l'+L}(l''||C^\nu||l)(k||C^\nu||l')\begin{Bmatrix} l'' & k & L \\ l' & l & \nu \end{Bmatrix},$$
$$e_\nu = (-)^{k+l'+L}(l''||C^\nu||l')(k||C^\nu||l)\begin{Bmatrix} l'' & k & L \\ l & l' & \nu \end{Bmatrix}. \quad (15)$$

Here, $(l||C^\nu||l')$ is the reduced matrix element of the spherical harmonic, multiplied by $[4\pi/(2\nu+1)]^{1/2}$, and

TABLE I. Auger transition probabilities to an initial 1s vacancy, in LS couplings, in terms of radial matrix elements $\{(nl)(n'l'), \nu, k\}$.

Final-state configuration		Term	Transition probability[a]
ns	$n's$	$^1S_0$; $^3S_1$	$\frac{1}{2}(2J+1)\,\alpha\,\lvert\{(ns)(n's),\,0,\,0\}\pm\{(n's)(ns),\,0,\,0\}\rvert^2$
ns	$n'p$	$^1P_1$; $^3P_{012}$	$\frac{1}{2}(2J+1)\,\lvert\{(ns)(n'p),\,0,\,1\}\pm\frac{1}{3}\{(n'p)(ns),\,1,\,1\}\rvert^2$
np	$n'p$	$^1S_0$; $^3S_1$	$\frac{1}{6}(2J+1)\,\alpha\,\lvert\{(np)(n'p),\,1,\,0\}\pm\{(n'p)(np),\,1,\,0\}\rvert^2$
		$^1D_2$; $^3D_{123}$	$\frac{1}{15}(2J+1)\,\alpha\,\lvert\{(np)(n'p),\,1,\,2\}\pm\{(n'p)(np),\,1,\,2\}\rvert^2$
ns	$n'd$	$^1D_2$; $^3D_{123}$	$\frac{1}{2}(2J+1)\,\lvert\{(ns)(n'd),\,0,\,2\}\pm\frac{1}{5}\{(n'd)(ns),\,2,\,2\}\rvert^2$
np	$n'd$	$^1P_1$; $^3P_{012}$	$\frac{1}{9}(2J+1)\,\lvert\{(np)(n'd),\,1,\,1\}\pm\frac{3}{5}\{(n'd)(np),\,2,\,1\}\rvert^2$
		$^1F_3$; $^3F_{234}$	$\frac{1}{14}(2J+1)\,\lvert\{(np)(n'd),\,1,\,3\}\pm\frac{3}{5}\{(n'd)(np),\,2,\,3\}\rvert^2$
ns	$n'f$	$^1F_3$; $^3F_{234}$	$\frac{1}{2}(2J+1)\,\lvert\{(ns)(n'f),\,0,\,3\}\pm\frac{1}{7}\{(n'f)(ns),\,3,3\}\rvert^2$
np	$n'f$	$^1D_2$; $^3D_{123}$	$\frac{1}{10}(2J+1)\,\lvert\{(np)(n'f),\,1,\,2\}\pm\frac{3}{7}\{(n'f)(np),\,3,2\}\rvert^2$
		$^1G_4$; $^3G_{345}$	$\frac{1}{27}(4J+2)\,\lvert\{(np)(n'f),\,1,\,4\}\pm\frac{3}{7}\{(n'f)(np),\,3,\,4\}\rvert^2$
nd	$n'd$	$^1S_0$; $^3S_1$	$\frac{1}{10}(2J+1)\,\alpha\,\lvert\{(nd)(n'd),\,2,0\}\pm\{(n'd)(nd),\,2,\,0\}\rvert^2$
		$^1D_2$; $^3D_{123}$	$\frac{1}{35}(2J+1)\,\alpha\,\lvert\{(nd)(n'd),\,2,\,2\}\pm\{(n'd)(nd),\,2,\,2\}\rvert^2$
		$^1G_4$; $^3G_{345}$	$\frac{1}{35}(2J+1)\,\alpha\,\lvert\{(nd)(n'd),\,2,\,4\}\pm\{(n'd)(nd),\,2,\,4\}\rvert^2$
nd	$n'f$	$^1P_1$; $^3P_{012}$	$\frac{1}{50}(6J+3)\,\lvert\{(nd)(n'f),\,2,\,1\}\pm\frac{5}{7}\{(n'f)(nd),\,3,\,1\}\rvert^2$
		$^1F_3$; $^3F_{234}$	$\frac{1}{75}(4J+2)\,\lvert\{(nd)(n'f),\,2,\,3\}\pm\frac{5}{7}\{(n'f)(nd),\,3,\,3\}\rvert^2$
		$^1H_5$; $^3H_{456}$	$\frac{1}{33}(2J+1)\,\lvert\{(nd)(n'f),\,2,\,5\}\pm\frac{5}{7}\{(n'f)(nd),\,3,\,5\}\rvert^2$

[a]Here, we have $\alpha\equiv\frac{1}{2}$ if $n=n'$, $\alpha\equiv 1$ if $n\neq n'$, and $\pm$ means + for singlet and − for triplet states.

$$\begin{Bmatrix} l_1 & l_2 & L \\ l_3 & l_4 & S \end{Bmatrix}$$

is the 6-j symbol.

In Table I, we list radiationless transition probabilities derived in Russell-Saunders coupling for all relevant transitions that fill an initial K-shell vacancy. The angular factors d_ν and e_ν have been derived through a computer program that includes 3-j and 6-j symbol subroutines.[33] Previously derived factors[6,22] are included for the sake of completeness.

F. Energies

The binding energies used in these calculations are taken from the compilation of Bearden and Burr.[34] Following Callan,[14,15] we use neutral-atom binding energies for $E_{n''l''}$ and E_{nl} (see Fig. 1 for notation). In order to take account of decreased screening due to inner-shell ionization, the binding energy of a neutral atom of the next-higher atomic number, $Z+1$, is taken for $E_{n'l'}$.

III. RESULTS AND DISCUSSION

A. Radiationless Transition Probabilities

The radiationless transition probabilities computed in the present work are summarized in Table II. The total radiationless K-level widths and the K-LL transition probabilities are compared in Figs. 2 and 3 with results from two other calculations. Of these, Callan's K-LL transition probabilities vary from our values only because of differences in screening and in level energies. To obtain total radiationless widths, Callan adjusted his K-LL transition probabilities with $(K\text{-}XY)/(K\text{-}LL)$ ratios calculated by Geffrion and Nadeau[35] from unscreened hydrogenic wave functions. McGuire's approach,[28] on the other hand, is very different from Callan's and our own: McGuire computed the quantity $-rV(r)$ for atoms with a K-shell vacancy by the approach of Herman and Skillman,[36] made a straight-line approximation to $-rV(r)$, and thus obtained a one-electron Schrödinger equation that could be solved exactly in terms of Whittaker functions for the radial part. This novel approach leads to excellent $(K\text{-}LX)/(K\text{-}LL)$ transition-probability ratios, as illustrated in Fig. 4. However, McGuire's fluorescence yields and total K widths agree somewhat less well with experiment, as indicated below.

B. K-Shell Fluorescence Yields

Auger and radiative K widths and fluorescence yields for elements from Ne through Yb are listed in Table III. For the purpose of comparison, re-

TABLE II. Calculated K Auger transition probabilities (in multiples of 10^{-3} a. u.)[a].

Element	$K-L_1L_1$	$K-L_1L_{23}$	$K-L_{23}L_{23}$	Total $K-LL$	$K-L_1M_1$	$K-L_1M_{23}$	$K-L_1M_{45}$	$K-L_{23}M_1$	$K-L_{23}M_{23}$	$K-L_{23}M_{45}$	Total $K-LM$	$K-L_1N_1$	$K-L_1N_{23}$	$K-L_1N_{45}$	$K-L_{23}N_1$	$K-L_{23}N_{23}$	$K-L_{23}N_{45}$	Total $K-LN$
$_{10}$Ne	3.397	4.151	0.950	8.498														
$_{12}$Mg	3.203	5.551	2.335	11.089	0.887			1.116			2.003							
$_{14}$Si	3.088	6.260	3.753	13.101	1.153	0.052		1.613	0.068		2.886							
$_{16}$S	3.003	6.781	5.035	14.819	1.258	0.199		1.900	0.289		3.646							
$_{18}$Ar	2.931	7.210	6.256	16.397	1.310	0.369		2.125	0.658		4.462							
$_{20}$Ca	2.881	7.293	7.212	17.386	1.373	0.596		2.193	1.163		5.325	0.239			0.414			0.653
$_{22}$Ti	2.832	7.482	8.078	18.392	1.382	0.681		2.279	1.458		5.800	0.230			0.437			0.667
$_{24}$Cr	2.790	7.620	8.816	19.226	1.373	0.730	0.001	2.350	1.673	0.005	6.132	0.221			0.442			0.663
$_{26}$Fe	2.757	7.759	9.463	19.979	1.377	0.770	0.003	2.413	1.865	0.012	6.440	0.210			0.441			0.651
$_{28}$Ni	2.756	7.866	10.049	20.671	1.370	0.798	0.005	2.466	2.031	0.025	6.695	0.200			0.438			0.638
$_{30}$Zn	2.704	7.696	10.583	21.256	1.367	0.823	0.005	2.517	2.182	0.030	6.924	0.190			0.432			0.622
$_{32}$Ge	2.688	8.012	11.007	21.707	1.370	0.879	0.011	2.514	2.420	0.062	7.256	0.267	0.005		0.604	0.015		0.891
$_{34}$Se	2.672	8.021	11.383	22.076	1.371	0.944	0.018	2.498	2.675	0.098	7.604	0.316	0.019		0.708	0.064		1.107
$_{36}$Kr	2.659	8.063	11.690	22.412	1.372	1.013	0.025	2.479	2.946	0.139	7.974	0.350	0.041		0.777	0.144		1.312
$_{38}$Sr	2.649	8.048	12.056	22.753	1.373	1.073	0.032	2.455	3.022	0.180	8.135	0.396	0.075		0.866	0.256		1.593
$_{40}$Zr	2.637	8.049	12.338	23.024	1.371	1.132	0.040	2.429	3.389	0.227	8.588	0.402	0.099		0.910	0.338		1.749
$_{42}$MO	2.626	8.049	12.581	23.256	1.369	1.182	0.047	2.405	3.591	0.271	8.865	0.438	0.118		0.936	0.407		1.899
$_{44}$Ru	2.615	8.052	12.821	23.488	1.365	1.228	0.054	2.380	3.779	0.317	9.123	0.450	0.135		0.953	0.469		2.007
$_{46}$Pd	2.605	8.052	13.031	23.688	1.362	1.269	0.061	2.359	3.949	0.360	9.360	0.459	0.151		0.965	0.525		2.100
$_{48}$Cd	2.596	8.056	13.236	23.888	1.359	1.305	0.069	2.339	4.106	0.406	9.584	0.465	0.165		0.973	0.578		2.181
$_{50}$Sn	2.588	8.056	13.416	24.060	1.356	1.342	0.076	2.319	4.257	0.448	9.798	0.475	0.187		0.983	0.656		2.301
$_{52}$Te	2.581	8.051	13.574	24.206	1.353	1.375	0.082	2.299	4.393	0.486	9.988	0.483	0.209		0.990	0.734		2.416
$_{54}$Xe	2.574	8.048	13.726	24.348	1.348	1.405	0.088	2.278	4.524	0.526	10.169	0.490	0.232		0.995	0.814		2.531
$_{56}$Ba	2.567	8.047	13.865	24.479	1.344	1.434	0.094	2.260	4.645	0.562	10.339	0.494	0.253		0.996	0.889		2.632
$_{58}$Ce	2.559	8.040	13.992	24.591	1.340	1.458	0.098	2.241	4.755	0.599	10.491	0.497	0.265		0.994	0.934		2.690
$_{60}$Nd	2.550	8.032	14.104	24.686	1.334	1.481	0.104	2.223	4.858	0.634	10.634	0.498	0.274		0.991	0.973		2.736
$_{65}$Tb	2.531	8.003	14.320	24.854	1.322	1.528	0.115	2.180	5.068	0.713	10.926	0.498	0.292	0.009	0.982	1.046	0.067	2.894
$_{70}$Yb	2.506	7.957	14.485	24.948	1.307	1.560	0.821	2.138	5.234	0.780	11.840	0.496	0.304	0.010	0.970	1.099	0.079	2.958

TABLE II. *Continued*

Element	$K-M_1M_1$	$K-M_1M_{23}$	$K-M_1M_{45}$	$K-M_{23}M_{23}$	$K-M_{23}M_{45}$	$K-M_{45}M_{45}$	Total $K-MM$	$K-M_1N_1$	$K-M_1N_{23}$	$K-M_{23}N_1$	$K-M_{23}N_{23}$	$K-M_{45}N_1$	$K-M_{45}N_{23}$	$K-M_{23}N_{45}$	$K-M_1N_{45}$	Total $K-MN$	Total all transitions
$_{10}$Ne																	8.498
$_{12}$Mg	0.059						0.059										13.151
$_{14}$Si	0.106	0.016		0.000			0.122										16.109
$_{16}$S	0.131	0.070		0.004			0.205										18.670
$_{18}$Ar	0.146	0.131		0.017			0.294										21.153
$_{20}$Ca	0.163	0.206		0.046			0.415	0.056		0.043						0.099	23.875
$_{22}$Ti	0.168	0.235		0.063			0.466	0.056		0.050						0.106	25.421
$_{24}$Cr	0.171	0.252	0.000	0.077	0.001	0.000	0.501	0.054		0.052		0.000				0.106	26.628
$_{26}$Fe	0.172	0.266	0.001	0.090	0.001	0.000	0.530	0.052		0.054		0.000				0.106	27.703
$_{28}$Ni	0.172	0.278	0.003	0.099	0.002	0.000	0.554	0.050		0.055		0.000				0.105	28.663
$_{30}$Zn	0.172	0.287	0.003	0.109	0.003	0.000	0.574	0.047		0.055		0.000				0.102	29.480
$_{32}$Ge	0.174	0.297	0.005	0.130	0.006	0.000	0.612	0.066	0.002	0.077	0.005	0.002	0.000			0.152	30.618
$_{34}$Se	0.176	0.312	0.008	0.154	0.009	0.000	0.659	0.079	0.007	0.094	0.007	0.003	0.000			0.190	31.636
$_{36}$Kr	0.177	0.327	0.011	0.179	0.014	0.000	0.708	0.088	0.015	0.108	0.017	0.005	0.001			0.234	32.640
$_{38}$Sr	0.178	0.341	0.014	0.204	0.019	0.000	0.756	0.101	0.027	0.126	0.031	0.006	0.001			0.292	33.529
$_{40}$Zr	0.179	0.353	0.016	0.228	0.025	0.000	0.801	0.108	0.034	0.137	0.044	0.008	0.003	0.000	0.000	0.334	34.496
$_{42}$Mo	0.179	0.364	0.019	0.251	0.031	0.001	0.845	0.113	0.039	0.146	0.054	0.009	0.004	0.000	0.000	0.365	35.230
$_{44}$Ru	0.179	0.373	0.020	0.274	0.037	0.001	0.884	0.116	0.044	0.154	0.066	0.011	0.004	0.000	0.000	0.395	35.897
$_{46}$Pd	0.179	0.382	0.023	0.293	0.043	0.001	0.921	0.118	0.048	0.160	0.070	0.012	0.005	0.000	0.000	0.419	36.488
$_{48}$Cd	0.179	0.388	0.025	0.313	0.050	0.001	0.956	0.121	0.052	0.165	0.086	0.014	0.007	0.001	0.000	0.446	37.019
$_{50}$Sn	0.178	0.394	0.026	0.331	0.057	0.002	0.988	0.123	0.057	0.171	0.099	0.015	0.008	0.002	0.000	0.475	37.622
$_{52}$Te	0.178	0.400	0.028	0.349	0.063	0.002	1.020	0.125	0.063	0.176	0.114	0.016	0.011	0.002	0.000	0.507	38.137
$_{54}$Xe	0.178	0.405	0.029	0.366	0.070	0.002	1.050	0.128	0.069	0.180	0.129	0.017	0.012	0.003	0.000	0.538	38.636
$_{56}$Ba	0.177	0.409	0.031	0.382	0.076	0.003	1.078	0.129	0.075	0.184	0.143	0.018	0.013	0.006	0.001	0.562	39.090
$_{58}$Ce	0.176	0.413	0.032	0.397	0.082	0.003	1.103	0.130	0.077	0.187	0.153	0.019	0.015	0.006	0.001	0.588	39.463
$_{60}$Nd	0.176	0.416	0.034	0.411	0.086	0.003	1.126	0.130	0.079	0.189	0.161	0.019	0.016	0.007	0.001	0.602	39.784
$_{65}$Tb	0.174	0.422	0.036	0.442	0.099	0.004	1.177	0.130	0.083	0.192	0.178	0.021	0.020	0.009	0.003	0.636	40.487
$_{70}$Yb	0.171	0.424	0.037	0.466	0.112	0.005	1.215	0.129	0.084	0.196	0.191	0.022	0.023	0.011	0.003	0.659	41.620

[a] 1 a.u. $= 4.134\times10^{16}\,\mathrm{sec}^{-1} = 27.212\,\mathrm{eV}/\hbar$

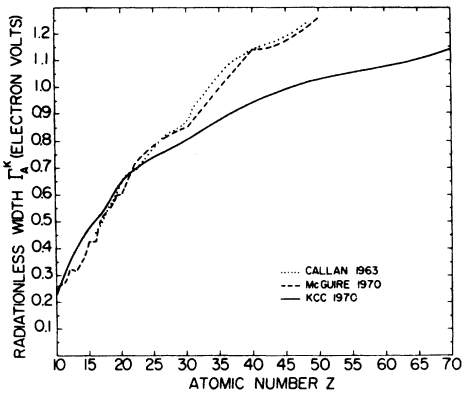

FIG. 2. Theoretical total Auger width of the 1s level, as a function of atomic number. The results of Callan's calculations are from Ref. 15, McGuire's are from Ref. 28, and KCC denotes the present work.

sults of Callan[15] and of McGuire[28] are also indicated. We furthermore list values of ω_K derived from a best fit[2,37] of the function[38,39]

$$\omega_K = \frac{(A+BZ+CZ^3)^4}{1+(A+BZ+CZ^3)^4} \tag{16}$$

to a critically selected and evaluated set of "most reliable" experimental results.[2] It should be noted, however, that this semiempirical curve fits the experimental data poorly below $Z \cong 20$. The present theoretical fluorescence yields, on the other hand, agree well with experiment down to $Z = 10$, as can be seen from Fig. 5. Also at high Z, the calculations agree quite closely with experiment. Neglect of relativistic corrections to the Auger transition probability causes this probability to be underestimated, and hence, our calculated values of ω_K are too high above $Z \cong 50$ (broken curve in Fig. 5). However, the excess is only slight, justifying our assumption that fluorescence yields for a rather wide range of atomic numbers can be derived from nonrelativistic Auger transition probabilities, as long as the radiative transition rates, which dominate at high Z, are calculated relativistically. Thus, the present results for ω_K agree better with experiment for $10 \leq Z \lesssim 65$ than the recent relativistic Hartree-Fock-Slater calculations of Bhalla, Ramsdale, and Rosner.[40]

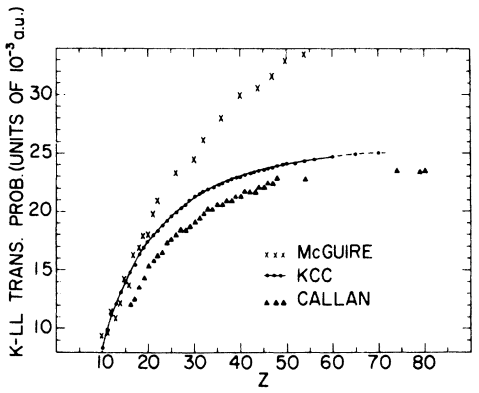

FIG. 3. Radiationless K-LL transition probability as a function of atomic number. McGuire's theoretical results are from Ref. 28, Callan's from Ref. 15, and KCC denotes the present work.

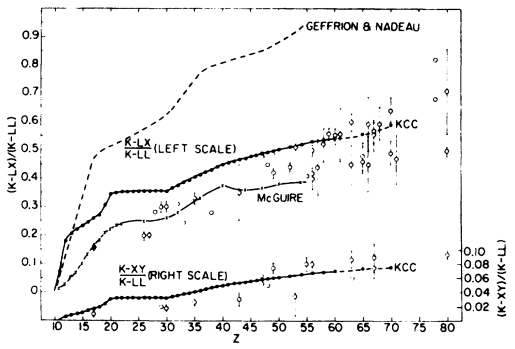

FIG. 4. Theoretical and experimental $(K\text{-}LX)/(K\text{-}LL)$ and $(K\text{-}XY)/(K\text{-}LL)$ Auger transition-probability ratios as a function of atomic number. Calculated ratios are from Geffrion and Nadeau (Ref. 35), McGuire (Ref. 28), and the present work (KCC). Measured relative intensities of the K Auger-electron groups are those assembled by P. Erman, J. Rossi, E. C. O. Bonacalza, and J. Miskel [Arkiv Fysik 26, 135 (1964)], except for the following: The Zn ratios are from J. B. Bellicard, A. Moussa, and S. K. Haynes, Nucl. Phys. 3, 307 (1956); the Co ratios are from J. B. Bellicard, A. Moussa, and S. K. Haynes, J. Phys. Radium 18, 115 (1957); the Te data are from W. R. Casey and R. G. Albridge Z. Physik 219, 216 (1969); while Ce and Nd ratios are those reported by B. B. D'Yakov and I. M. Rogachev, Bull. Acad. Sci. USSR, Phys. Ser. 26, 191 (1962).

It is interesting to note that, in spite of large differences in calculated radiationless transition probabilities (see Fig. 2 and Table III), fluorescence yields computed in all but the earliest work are rather consistent, as illustrated in Fig. 6. This curious effect arises because those calculations that lead to exceptionally large Auger transition probabilities also appear to result in large radiative transition probabilities, as can be seen from Table III. A more sensitive test of various approaches can therefore be sought in a comparison of experimental and calculated *total* 1s-level widths.

C. Total K-Level Widths

Experimental information on the total K-level width $\Gamma^K = \Gamma_A^K + \Gamma_R^K$ can be derived from linewidth determinations of x-ray emission lines. After correcting for instrumental contributions to $K\alpha_1$ and $K\alpha_2$ linewidths, L_3 and L_2 level widths are subtracted to find Γ^K. The information is scarce

TABLE III. K-shell radiationless widths Γ_A^K, radiative widths Γ_R^K, and fluorescence yields ω_K.

Element	Radiationless width Γ_A^K (eV)			Radiative width Γ_R^K (eV)			Fluorescence yield ω_K			
	Callan[a]	McGuire[b]	This work	Callan[a]	McGuire[b]	Scofield[c]	Callan[a]	McGuire[b]	Semi-empirical[d]	This work
10^{Ne}		0.243	0.231		0.0045	0.0048		0.0182	0.012	0.0204
11^{Na}		0.264	0.289		0.0071	0.0071		0.0260	0.017	0.0240
12^{Mg}		0.314	0.358		0.0109	0.0100		0.0336	0.025	0.0272
13^{Al}		0.318	0.400		0.0144	0.0138		0.0412	0.0336	0.0333
14^{Si}		0.346	0.438		0.0217	0.0202		0.0592	0.0447	0.0441
15^{P}		0.390	0.475		0.0313	0.0288		0.0743	0.0581	0.0572
16^{S}	0.46	0.425	0.508	0.05	0.0420	0.0398	0.098	0.0899	0.0739	0.0727
17^{Cl}	0.50	0.486	0.536	0.06	0.0586	0.0540	0.117	0.108	0.0922	0.0915
18^{Ar}	0.56	0.531	0.576	0.09	0.0769	0.0717	0.138	0.126	0.113	0.111
19^{K}	0.60	0.576	0.611	0.11	0.101	0.0933	0.155	0.149	0.136	0.132
20^{Ca}	0.66	0.593	0.650	0.13	0.129	0.119	0.165	0.177	0.162	0.155
21^{Sc}	0.68	0.604	0.671	0.16	0.157	0.150	0.190	0.205	0.190	0.183
22^{Ti}	0.70	0.676	0.692	0.19	0.206	0.186	0.213	0.233	0.220	0.212
23^{V}	0.72		0.710	0.23		0.228	0.242		0.251	0.243
24^{Cr}	0.75		0.725	0.28		0.276	0.272		0.284	0.276
25^{Mn}	0.78		0.740	0.32		0.333	0.291		0.317	0.310
26^{Fe}	0.81	0.771	0.754	0.38	0.445	0.396	0.319	0.364	0.351	0.344
27^{Co}	0.83		0.768	0.44		0.469	0.346		0.386	0.379
28^{Ni}	0.84		0.780	0.51		0.551	0.378		0.419	0.414
28^{Cu}	0.86		0.791	0.59		0.643	0.407		0.453	0.448
30^{Zn}	0.88	0.831	0.802	0.67	0.851	0.747	0.438	0.499	0.485	0.482
31^{Ga}	0.93		0.818	0.82		0.864	0.469		0.517	0.514
32^{Ge}	0.96	0.882	0.833	1.00	1.13	0.996	0.510		0.547	0.545
33^{As}	0.99		0.848	1.20		1.142	0.548		0.576	0.574
34^{Se}	1.02		0.861	1.44		1.305	0.585		0.603	0.602
35^{Br}	1.05		0.875	1.77		1.486	0.628		0.629	0.629
35^{Kr}	1.08	0.994	0.888	2.10	1.95	1.686	0.660	0.659	0.654	0.655
37^{Rb}	1.10		0.902	2.34		1.905	0.680		0.677	0.679
38^{Sr}	1.11		0.912	2.61		2.144	0.702		0.698	0.702
39^{Y}	1.13		0.928	2.89		2.405	0.719		0.718	0.722
40^{Zr}	1.14	1.10	0.939	3.20	3.21	2.688	0.737	0.740	0.737	0.741
41^{Nb}	1.15		0.950	3.53		2.995	0.754		0.754	0.759
42^{Mo}	1.16		0.959	3.89		3.328	0.770		0.770	0.776
43^{Tc}	1.17		0.968	4.27		3.687	0.785		0.785	0.792
44^{Ru}	1.18	1.13	0.977	4.69	4.81	4.075	0.799	0.806	0.799	0.807
45^{Rh}	1.19		0.985	5.13		4.493	0.812		0.811	0.820
46^{Pd}	1.21		0.993	5.60		4.940	0.822		0.823	0.833
47^{Ag}	1.22	1.17	1.000	6.10	6.40	5.423	0.833	0.842	0.834	0.844
48^{Cd}	1.24		1.007	6.64		5.940	0.843		0.844	0.855
49^{In}			1.016			6.494			0.854	0.865
50^{Sn}		1.23	1.024		8.48	7.089		0.871	0.862	0.874
52^{Te}			1.038			8.402			0.878	0.890
54^{Xe}			1.051			9.894			0.891	0.904
56^{Ba}			1.064			11.57			0.903	0.916
58^{Ce}			1.074			13.44			0.912	0.926
60^{Nd}			1.082			15.52			0.921	0.935
65^{Tb}			1.102			21.75			0.938	0.952
70^{Yb}			1.133			29.65			0.950	0.963

[a]E. J. Callan, Ref. 15.

[b]E. J. McGuire, Ref. 28.

[c]J. H. Scofield, Ref. 3. These radiative widths agree to within at least three significant figures with the relativistic calculation of atomic x-ray transition rates recently published by H. R. Rosner and C. P. Bhalla [Z. Physik 231, 347 (1970)].

[d]Fit of Burhop's semiempirical relation [Eq. (16)] to selected "most reliable" experimental results (Refs. 2 and 37).

and widely scattered, but fortunately has been collected by Leisi *et al.*,[41] who find that Γ^K is well represented by the expression

$$\Gamma^K = 1.73 \times Z^{3.93} \times 10^{-6}\ \text{eV} \qquad (17)$$

for $Z > 40$, within the errors of measurement.

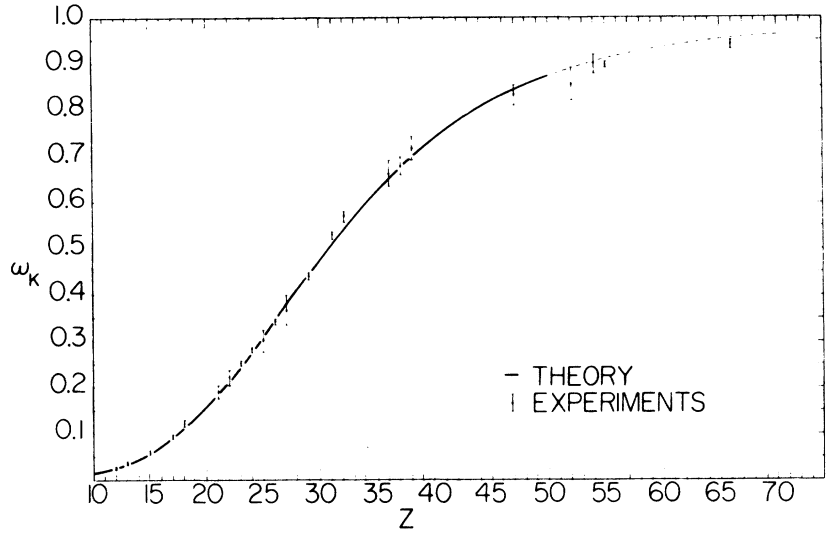

FIG. 5. Theoretical K-shell fluorescence yield from the present work, as a function of atomic number. The data points are "most reliable" critically evaluated experimental results from Ref. 2.

In Table IV, we compare Callan's,[15] McGuire's,[28] and the present total K-level widths with Leisi's semiempirical values. The lower Γ^K values of the present calculation are seen to agree best with experimental widths.

D. Byrne-Howarth Plot

Because it is difficult to fit Burhop's relation [Eq. (16)] over the entire range of atomic numbers, Byrne and Howarth[42] have recently suggested the alternative semiempirical expression

$$\ln[1-\omega_K)/\omega_K] = -m\ln Z + \ln\alpha, \tag{18}$$

according to which a plot of $\ln[(1-\omega_K)/\omega_K]$ against $\ln Z$ should give a straight line of slope $-m$ and intercept $\ln\alpha$. Such a plot of the results of the present calculation is shown in Fig. 7. For $15 \leq Z \leq 70$, the theoretical fluorescence yields can be least-squares fitted by a straight line with $m = 3.94$ and $\ln\alpha = 13.5$.

ACKNOWLEDGMENTS

We wish to thank Dr. G. D. Mahan of the University of Oregon for helpful conversations and Dr. E. J. Callan of the Aerospace Research Laboratories, Wright-Patterson Air Force Base, for correspondence on the subject of these calculations. Dr. J. H. Scofield of the Lawrence Radiation Laboratory, Livermore, kindly made a complete list of his radiative transition probabilities available to us. We are grateful to Dr. W. Bambynek of the Bureau Central de Mesures Nucléaires in Geel, Belgium, for granting us permission to quote the results of his semiempirical fit to best experimental values of ω_K. We thank Dr. E. J. McGuire of the Sandia Laboratories for making his results available to us in advance of publication.

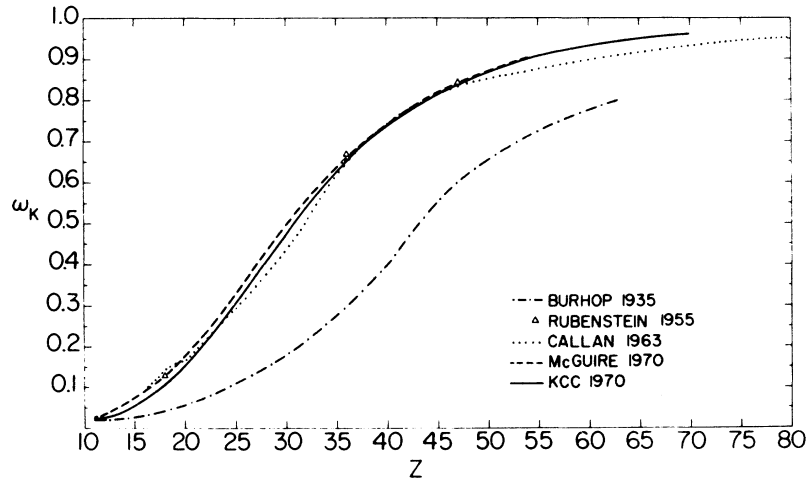

FIG. 6. Theoretical K-shell fluorescence yield as a function of atomic number, according to various authors: Burhop (Ref. 12), Rubenstein (Ref. 22), Callan (Ref. 15), McGuire (Ref. 28), and KCC (the present work).

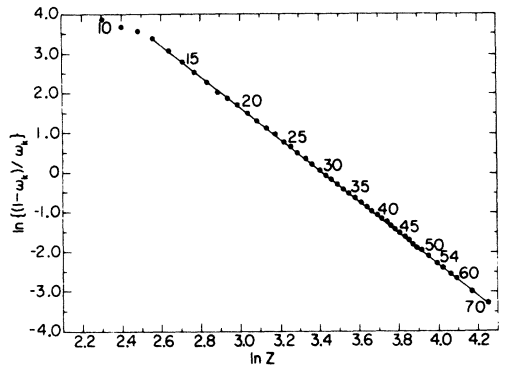

FIG. 7. Byrne-Howarth plot of theoretical K-shell fluorescence yields computed in the present work. Over the range $13 \leq Z \leq 70$, the results closely fit a straight line.

Miss Louise K. Permann and Miss Margaret C.-K. Yeung helped with some of the computations. One of us (B. C.) wishes to express his appreciation to Dr. Hans Mark and Dr. Eugene Goldberg, "E"-Division Leader, for their hospitality during 1968–69 at the Lawrence Radiation Laboratory, Livermore, where some of this work was done.

TABLE IV Comparison of total K-level widths.

Atomic number	Γ^K (eV) Callan[a]	McGuire[b]	This work	Experiment[c]
40	4.34	4.58	3.63	3.42
41	4.68		3.95	3.77
42	5.05		4.29	4.14
43	5.44		4.66	4.55
44	5.87	6.23	5.05	4.98
45	6.32		5.48	5.43
46	6.81		5.93	5.93
47	7.32	7.85	6.42	6.45
48	7.88		6.95	7.00
49			7.51	7.60
50		9.96	8.12	8.22

[a]E. J. Callan, Ref. 15.
[b]E. J. McGuire, Ref. 28.
[c]Semiempirical values of H. J. Leisi *et al.*, Ref. 41.

APPENDIX A: RADIAL MATRIX ELEMENTS

With nonrelativistic hydrogenic bound-state wave functions and the continuum wave function of Eq. (5), the radial matrix element becomes[33]

$$\{(n''l'')|\,(nl)(n'l'),\nu,k\} = (e^2/\hbar^2)(m/\hbar)^{1/2} A_{n''l''} A_{n'l'} A_{nl}$$

$$\times \sum_{s''=0}^{n''-l''-1} \sum_{s'=0}^{n'-l'-1} \sum_{s=0}^{n-l-1} B_{n''l''s''} B_{n'l's'} B_{nls} \left\{ \frac{(l''+s''+l+s+2+\nu)!}{[\frac{1}{2}(c_1+c_2)]^{l''+s''+l+s+3+\nu}} \int_0^\infty e^{-(c_3/2)x} x^{l''+s''+1-\nu} Q(x,\eta,k)\,dx \right.$$

$$- (l''+s''+l+s+2+\nu)! \sum_{j=1}^{l''+s''+l+s+3+\nu} \frac{\int_0^\infty e^{-[(c_1+c_2+c_3)/2]x} x^{l''+s''+l'+s'+l+s+4-j} Q(x,\eta,k)\,dx}{[\frac{1}{2}(c_1+c_2)]^j (l''+s''+l+s+3+\nu-j)!}$$

$$\left. + (l''+s''+l+s+1-\nu)! \sum_{j=1}^{l''+s''+l+s+2-\nu} \frac{\int_0^\infty e^{-[(c_1+c_2+c_3)/2]x} x^{l''+s''+l'+s'+l+s+4-j} Q(x,\eta,k)\,dx}{[\frac{1}{2}(c_1+c_2)]^j (l''+s''+l+s+2-\nu-j)!} \right\}, \quad \text{(A1)}$$

where

$$A_{nl} = -\left(\frac{(n-l-1)!}{2n[(n+l)!]^3}\right)^{1/2} \left(\frac{2Z}{na\kappa}\right)^{l+3/2},$$

$$B_{nls} = (-)^{s+1} \left(\frac{[(n+l)!]^2}{(2l+1+s)!\,s!\,(n-1-l-s)!}\right) \left(\frac{2Z}{na\kappa}\right)^s,$$

$$x = \kappa r, \quad \kappa = \left(\frac{E_{n''} - E_n - E_{n'}}{13.602}\right)^{1/2}, \quad (E \text{ in eV}),$$

$$c_1 = \left(\frac{2Z''}{n''a\kappa}\right), \quad c_2 = \left(\frac{2Z}{na\kappa}\right), \quad c_3 = \left(\frac{2Z'}{n'a\kappa}\right), \qquad \eta = Z'/\kappa. \quad \text{(A2)}$$

The Z's are effective charges and the E's absolute values of the binding energies in the respective states, while a is the Bohr radius. The function Q, which occurs in the continuum wave function, is defined as follows:

$$Q(x,\eta,k) \equiv \frac{2^{k+1}}{(2k+1)!}\, e^{\pi\eta/2} \left|\, \Gamma(k+1+i\eta) \right|$$

$$\times x^k e^{-ix}\,{}_1F_1(k+1+i\eta;\ 2k+2;\ 2ix)\,. \qquad \text{(A3)}$$

The integrals in Eq. (10), involving the confluent hypergeometric function ${}_1F_1(a;b;cx)$ can be evaluated analytically as follows:

$$\int_0^\infty e^{-qx} x^p Q(x,\eta,k)\,dx$$

$$= \frac{2^{k+1}}{(2k+1)} e^{\pi\eta/2} \left|\Gamma(k+1+i\eta)\right| \frac{(p+k)!}{(i+q)^{p+k+1}}$$

$$\times\ {}_2F_1\left(k+1+i\eta,\ p+k+1;\ 2k+2;\ \frac{2i}{i+q}\right). \qquad \text{(A4)}$$

The following general result is found for the radial matrix element[33]:

$$\{(n''l'')|\,(nl)(n'l'),\nu,k\} = A_{n''l''}A_{n'l'}A_{nl}\sum_{s''=0}^{n''-l''-1}\sum_{s'=0}^{n'-l'-1}\sum_{s=0}^{n-l-1} B_{n''l''s''}B_{n'l's'}B_{nls}\left\{\frac{(l''+s''+l+s+2+\nu)!}{[\frac{1}{2}(c_1+c_2)]^{l''+s''+l+s+3+\nu}}\,P(l',s',k)\right.$$

$$-(l''+s''+l+s+2+\nu)!\sum_{j=1}^{l''+s''+l+s+3+\nu}\frac{P_j}{[\frac{1}{2}(c_1+c_2)]^j(l''+s''+l+s+3+\nu-j)!}$$

$$\left.+(l''+s''+l+s+1-\nu)!\sum_{j=1}^{l''+s''+l+s+2-\nu}\frac{P_j}{[\frac{1}{2}(c_1+c_2)]^j(l''+s''+l+s+2-\nu-j)!}\right\}, \qquad \text{(A5)}$$

where

$$P(l',s',k) = G(k,\eta)\frac{(l'+s'+k+1-\nu)!}{(\frac{1}{2}c_3+i)^{l'+s'+k+2-\nu}}\,{}_2F_1(k+1+i\eta,\ l'+s'+k+2-\nu;\ 2k+2;\ 2i/(\tfrac{1}{2}c_3+i)\ , \qquad \text{(A6)}$$

$$P_j = G(k,\eta)\frac{(l''+s''+l'+s'+l+s+k+4-j)!}{[\frac{1}{2}(c_1+c_2+c_3)+i]^{l''+s''+l'+s'+l+s+k+5-j}}$$

$$\times\,{}_2F_1(k+1+i\eta,\ l''+s''+l'+s'+l+s+k+5-j;\ 2k+2;\ \frac{2i}{[\frac{1}{2}(c_1+c_2+c_3)+i]})\ , \qquad \text{(A7)}$$

$$G(k,\eta) = [2^{k+1}/(2k+1)!]\,e^{\pi\eta/2}\left|\Gamma(k+1+i\eta)\right|. \qquad \text{(A8)}$$

The expressions are given in atomic units ($e=\hbar=m=1$). The ordinary hypergeometric functions of complex arguments ${}_2F_1$ which occur in the matrix elements can be computed by the matrix method of Callan[16] or they can be constructed[33] with the aid of Gauss's relations for contiguous functions.[43]

APPENDIX B: RELATION BETWEEN WAVE FUNCTIONS IN j-j AND LS COUPLING

The j-j wave functions are given in terms of the LS wave functions by[32]

$$\psi_A(n_a l_a j_a,\ n_b l_b j_b;\ JM)$$

$$= \sum_{SL}[(2S+1)(2L+1)(2j_a+1)(2j_b+1)]^{1/2}$$

$$\times \begin{Bmatrix} \frac{1}{2} & l_a & j_a \\ \frac{1}{2} & l_b & j_b \\ S & L & J \end{Bmatrix} \psi_A(n_a l_a;\ n_b l_b;\ SLJM, \qquad \text{(B1)}$$

where

$$\begin{Bmatrix} \frac{1}{2} & l_a & j_a \\ \frac{1}{2} & l_b & j_b \\ S & L & J \end{Bmatrix}$$

is the 9-j symbol.

From the relation between the absolute squared values of the matrix elements of e^2/r_{12} in the two coupling schemes

$$\left|\langle n_a'l_a'j_a',\ n_b'l_b'j_b';\ JM|\,e^2/r_{12}\,|\,n_a l_a j_a,\ n_b l_b j_b;\ JM\rangle\right|^2 = \sum_{S,L,S',L'}[(2S+1)(2L+1)(2S'+1)](2L'+1)(2j_a'+1)$$

$$\times\,(2j_b'+1)(2j_a+1)(2j_b+1)]\begin{Bmatrix} \frac{1}{2} & l_a' & j_a' \\ \frac{1}{2} & l_b' & j_b' \\ \frac{1}{2} & L' & J \end{Bmatrix}\begin{Bmatrix} \frac{1}{2} & l_a & j_a \\ \frac{1}{2} & l_b & j_b \\ S' & L' & J \end{Bmatrix}\begin{Bmatrix} \frac{1}{2} & l_a' & j_a' \\ \frac{1}{2} & l_b' & j_b' \\ S & L & J \end{Bmatrix}\begin{Bmatrix} \frac{1}{2} & l_a & j_a \\ \frac{1}{2} & l_b & j_b \\ S & L & J \end{Bmatrix}$$

$$\times \langle n_a' l_a', n_b' l_b';\ SLJM \left| e^2/r_{12} \right| n_a l_a, n_b l_b;\ SLJM \rangle \langle n_a' l_a', n_b' l_b';\ S'L'JM \left| e^2/r_{12} \right| n_a l_a, n_b l_b;\ S'L'JM \rangle , \tag{B2}$$

it can readily be shown, by summing both sides over j_a, j_b, l_b', j_b', J, and M, that

$$w = \frac{1}{2j_a'+1} \sum_J (2J+1) \sum_{l_b, j_b} \sum_{j_a, j_b} \left| \langle n_a' l_a' j_a', n_b' l_b' j_b';\ J \left| \frac{e^2}{r_{12}} \right| n_a l_a j_a, n_b l_b j_b;\ J \rangle \right|^2$$

$$= \frac{1}{2(2l_a'+1)} \sum_{S,L} (2S+1)(2L+1) \sum_{l_b} \left| \langle n_a' l_a', n_b' l_b';\ SL \left| \frac{e^2}{r_{12}} \right| n_a l_a, n_b l_b;\ SL \rangle \right|^2 . \tag{B3}$$

Thus, if the initial vacancy (denoted by quantum numbers n_a', l_a', and j_a') has different n_a', l_a' from one of the vacancies appearing in the final-state configuration, as in radiationless transitions of the type X-YZ, then the total transition rate can be evaluated either in j-j or in LS coupling. On the other hand, if $n_a' = n_a$ and $l_a' = l_a$, as can happen in certain transitions of the X-XY type (e.g., L_2-L_3X), the summation over j_a on the left-hand side of Eq. (B2) cannot be performed, and the right-hand side of Eq. (B2) does not reduce to the simple expression given by the right-hand side of Eq. (B3). In such cases, it is easier to evaluate the total transition rate in j-j coupling:

$$w = \frac{1}{2j_a'+1} \sum_J (2J+1) \times \sum_{l_b j_b j_b} \left| \langle n_a' l_a' j_a', n_b' l_b' j_b';\ J \left| \frac{e^2}{r_{12}} \right| n_a l_a j_a, n_b l_b j_b;\ J \rangle \right|^2 . \tag{B4}$$

In other words, calculating a transition rate of the M_2-M_3X type, for example, in LS coupling would lead to the wrong answer, because included in the rate would be processes of the type $\langle 3p_{1/2}, n_b' l_b' j_b';\ J \left| e^2/r_{12} \right| 3p_{1/2}, n_b l_b j_b;\ J \rangle$, which clearly do not occur.

*Work supported in part by the U. S. Atomic Energy Commission.

[1]R. W. Fink, R. C. Jopson, Hans Mark, and C. D. Swift, Rev. Mod. Phys. 38, 513 (1966).

[2]W. Bambynek, B. Crasemann, R. W. Fink, H. -U. Freund, Hans Mark, R. E. Price, P. Venugopala Rao, and C. D. Swift (unpublished).

[3]J. H. Scofield, Phys. Rev. 179, 9 (1969).

[4]V. O. Kostroun, M. H. Chen, and B. Crasemann (unpublished).

[5]G. Wentzel, Z. Physik 43, 524 (1927).

[6]W. N. Asaad and E. H. S. Burhop, Proc. Phys. Soc. (London) 71, 369 (1958).

[7]E. U. Condon and G. H. Shortley, *The Theory of Atomic Spectra* (Cambridge U. P., Cambridge, England, 1953), Chap. XII.

[8]V. P. Sachenko and V. F. Demekhin, Izv. Akad. Nauk SSSR Ser. Fiz. 31, 942 (1967)[Bull. Acad. Sci. USSR, Phys. Ser. 31, 957 (1967)].

[9]V. P. Sachenko and E. V. Burtsev, Izv. Akad. Nauk SSSR Ser. Fiz. 31, 980 (1967)[Bull. Acad. Sci. USSR, Phys. Ser. 31, 980 (1967)].

[10]J. R. Oppenheimer, Z. Physik 55, 725 (1929).

[11]J. A. Gaunt, Phil. Trans. Roy. Soc. London A229, 163 (1930).

[12]E. H. S. Burhop, Proc. Roy. Soc. (London) A148, 272 (1935).

[13]See, for example, H. A. Bethe and E. E. Salpeter, *Quantum Mechanics of One- and Two-Electron Atoms* (Springer, Berlin, 1957), Chap. 1.

[14]E. J. Callan, Phys. Rev. 124, 793 (1961).

[15]E. J. Callan, in *Role of Atomic Electrons in Nuclear Transformations* (Nuclear Energy Information Center, Warsaw, 1963), Vol. 3, p. 419.

[16]E. J. Callan, P. Nikolai, and W. L. McDavid, in *Atomic Collision Processes*, edited by M. R. C. McDowell (North-Holland, Amsterdam, 1964), p. 348.

[17]In Ref. 15, p. 398.

[18]E. J. Callan, Rev. Modern Phys. 35, 524 (1963).

[19]H. S. W. Massey and E. H. S. Burhop, Proc. Roy. Soc. (London) A153, 661 (1936).

[20]D. Chattarji and B. Talukdar, Phys. Rev. 174, 44 (1968).

[21]B. Talukdar and D. Chattarji, Phys. Rev. A 1, 33 (1970).

[22]R. A. Rubenstein and J. N. Snyder, Phys. Rev. 97, 1653 (1955); R. A. Rubenstein, thesis, University of Illinois, 1955 (unpublished).

[23]W. N. Asaad, Proc. Roy. Soc. (London) 249, 555 (1959).

[24]M. A. Listengarten, Izv. Akad. Nauk SSSR Ser. Fiz. 25, 792 (1961)[Bull. Acad. Sci. USSR, Phys. Ser. 25, 803 (1961)].

[25]M. A. Listengarten, Izv. Akad. Nauk SSSR Ser. Fiz. 26, 182 (1962)[Bull. Acad. Sci. USSR, Phys. Ser. 26, 182 (1962)].

[26]W. Mehlhorn, Z. Physik 208, 1 (1968).

[27]E. J. McGuire, Phys. Rev. 185, 1 (1969).

[28]E. J. McGuire, Phys. Rev. A 2, 273 (1970).

[29]W. Gordon, Z. Physik 48, 180 (1928).

[30]D. Hartree, *The Calculation of Atomic Structures* (Wiley, New York, 1957), Chap. 7.

[31]C. Froese, University of British Columbia, 1966 (unpublished).

[32]A deShalit and I. Talmi, *Nuclear Shell Theory* (Academic, New York, 1963), Chaps. 19–21.

[33]V. O. Kostroun, Ph.D. thesis, University of Oregon, 1968 (unpublished).

[34]J. A. Bearden and A. F. Burr, Rev. Mod. Phys. 39, 125 (1967).

[35]C. Geffrion and G. Nadeau, U. S. Air Force Office of Scientific Research, Research Report No. TR 59–145, 1959 (unpublished).

[36]F. Herman and S. Skillman, *Atomic Structure Cal-*

culations (Prentice-Hall, Englewood Cliffs, N. J., 1963).
[37]W. Bambynek and R. W. Fink (private communication).
[38]E. H. S. Burhop, J. Phys. Radium 16, 625 (1955).
[39]J. Laberrigue-Frolow and P. Radvanyi, J. Phys. Radium 17, 944 (1956).
[40]C. P. Bhalla, D. J. Ramsdale, and H. R. Rosner, Phys. Letters 31A, 122 (1970).
[41]H. J. Leisi, J. H. Brunner, C. F. Perdrisat, and P. Scherrer, Helv. Phys. Acta 34, 161 (1961).
[42]J. Byrne and N. Howarth, J. Phys. B 3, 280 (1970).
[43]F. Oberhettinger, in *Handbook of Mathematical Functions*, edited by M. Abramowitz and I. A. Stegun, Applied Mathematics Series 55 (Natl. Bur. Std. U. S. GPO, Washington, D. C., 1964), Chap. 15.

PHYSICAL REVIEW A VOLUME 3, NUMBER 2 FEBRUARY 1971

Quadrupole Crystalline Electric Field Shielding and Antishielding Factors at Some Rare-Earth and Heavy Ions

R. P. Gupta,* B. K. Rao,† and S. K. Sen
Department of Physics, University of Manitoba, Winnipeg 19, Canada
(Received 3 August 1970)

We report the results of calculations of Sternheimer crystalline electric field shielding and antishielding factors for Pr^{3+}, Tm^{3+}, W^{+}, and Au^{+} ions at all the core electronic sites, in addition to the unfilled valence electron site and the nuclear site of each ion. The calculations take into account the effect of polarization of all the closed shells within the ions, including the exchange interaction terms. Mann's relativistically corrected Hartree-Fock (HF) wave functions were used in the computations. Our calculations thus extend and improve upon the previous calculations by Sternheimer and others who did the computations for rare-earth ions at the location of the $4f$ electron and at the nuclear site only. Our values of shielding and antishielding factors λs at the location of the $4f$ electron and at the nuclear site for Pr^{3+} and Tm^{3+} ions agree well with previous calculations and measurements. The possibility of experimentally determining the quadrupole splittings of the atomic-core level by the recently developed technique of electron spectroscopy for chemical analysis (ESCA), which underlines the great significance of these calculations, is discussed.

I. INTRODUCTION

It has been of considerable interest to estimate the Sternheimer shielding parameters at the $4f$-electron site and the antishielding parameters at the nuclear site in rare-earth ions.[1-3] The electric field at any location within the ion is known in terms of these parameters when the field produced at the site of the ion by the ligands surrounding the ion and by other rare-earth ions in the crystal is given. However, the calculation of crystalline-electric field (CEF) parameters, defining the field, is a formidable task except for the simple cases of high-symmetry crystals.[4] Since the CEF parameter A_2^0 enters directly in the expression for the hyperfine energy splitting of nuclear levels, an experimental determination of A_2^0 was always sought. The spectroscopic measurements[5] gave information about A_2^0 coupled with the Sternheimer shielding parameter. Thus, an accurate knowledge of Sternheimer shielding is necessary to determine the value of A_2^0 from the experiments. Recent development of high-resolution techniques, such as electron spectroscopy for chemical analysis (ESCA)[6] has made it possible to measure very small splittings of the electronic energy levels of the order of 0.5 eV. It has been suggested by Sen[7] that the splitting of some $p_{3/2}$ electronic states should be measurable in some compounds of heavier elements. The splitting of $5p_{3/2}$ and $4p_{3/2}$ levels has recently been observed in compounds of Au, Th, U, Pu, and Np by Novakov and Hollander.[8] In view of these facts it seemed necessary to carry out calculations of the Sternheimer parameters for various electronic sites in rare-earth and heavy ions. We report here the Sternheimer parameters (to be denoted by λ) for W^{+}, Au^{+}, Pr^{3+}, and Tm^{3+} ions at all the core-electronic sites, as well as at the nuclear site of each ion. As a by-product of these calculations, electronic quadrupole polarizabilities[9] for the ions were obtained. These are also reported here.

For W^{+} we have calculated $\lambda_{5d} = 0.110$ and λ_{nucl} (γ_∞ in Sternheimer's notation) $= -56.8$; for Au^{+}, $\lambda_{\text{nucl}} = -74.2$; for Pr^{3+}, λ_{4f} (σ_2 in Sternheimer's notation) $= 0.745$ and $\lambda_{\text{nucl}} = -84.8$; and for Tm^{3+}, $\lambda_{4f} = 0.601$ and $\lambda_{\text{nucl}} = -72.9$. The λ's here include the effect of polarization of all the cores, as well as exchange interaction terms. Mann's[10] relativistically corrected Hartree-Fock (HF) wave functions were used in all the calculations. The results for Pr^{3+} and Tm^{3+} compare well with other previous